

A Transit Dish Design for High-Redshift 21cm Intensity Mapping Experiments

ABSTRACT

1. Introduction

- importance of frequency smoothness
- collecting area

2. Background

- τ -modes, wedge, EoR window
- geometric interpretation of τ -modes

3. Geometric Constraints

- first principles of EoR window, how that maps to a specification for design
- cost analysis
- critically constrained design
- symmetric on-axis parabaloid, for reasons of symmetry in polarization response

4. Design and Construction

4.1. bent pipes as approximation to parabola

The construction method is based on the use of a reasonably stiff spar supported at a few points as a low-pass spatial filter. Additionally, a moment-loaded beam naturally attains a parabolic shape, depending on the loading, the moment of intertia and the material's Young's modulus (see *e.g.* [http://ruina.tam.cornell.edu/Courses/ME4730/Rand4770 Vibrations/BeamFormulas.pdf](http://ruina.tam.cornell.edu/Courses/ME4730/Rand4770%20Vibrations/BeamFormulas.pdf)). In this instance we fix the angle at the rim (r_e) of 7m and at a hub radius (r_h) of about 45 cm, so

between those two points, the effective angle is $(r_e - r_h)/(2F)$, where F is the focal length (4.5m). Equating that angle to the angle of the cantilevered beam (using scenario 5 of the web-site) we find

$$y = \left(\frac{r_e - r_h}{L} \right) \frac{x^2}{4F} \equiv \frac{x^2}{4F_e} \quad (1)$$

where L is the length of the beam. Note that we do not contend that this figure over the entire length of the actual beam achieves this, but merely that if properly held and loaded it tends to the right shape. Furthermore, we see that the parabola will tend to have a larger focal length than desired (about 10% for HERA) unless we compensate by modifying the end angle of the spar by setting it to $(L + r_h)/(2F)$.

In our construction, we hold the spar at three locations at the proper location and angle and then rely on the fairly stiff spar to "filter" out any higher frequency ripples and on the physics to give us the overall general shape.

Fig. 1.— THIS FIGURE SHOWS THE ANALYSIS ON PARABOLA

Fig. 2.— THIS FIGURE SHOWS THE PHOTGRAMMRY ANALYSIS

4.2. faceting

The construction of the surface stretches mesh panels over adjacent spars, so the surface is not a true paraboloid but rather a faceted parabola, although note that the construction does pull down the mesh mid-panel to both better approximate a paraboloid as well as to hold the mesh.

If we assume an actual faceted parabola (*i.e.* the mesh is perfectly flat between adjacent spars) we can calculate the rms deviation from a paraboloid for various spar configurations. For this antenna, we chose 12 spars out to 1.45m, then transitioning to 24 spars. Choosing just 12 spars all the way out to the rim yields an rms of 6.9cm (corresponding to a Ruze loss of almost 18% at 150 MHz), as opposed to 1.7cm (for about 1 % loss).

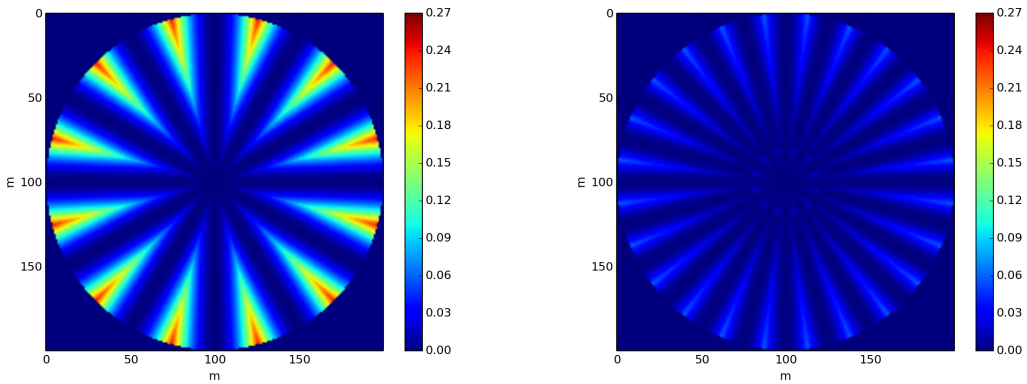


Fig. 3.— Contour plots of the facet deviations from a paraboloid for 12 spars (left) and the 12-to-24 spar design (right).

4.3. shielding

The panels across the dish surface are made out of 6 different dimensions of galvanized wire cloth $\frac{1}{4}$ "; employing different dimensions at different heights to reduce the surface bumps produced during installation.

4.4. splash cone

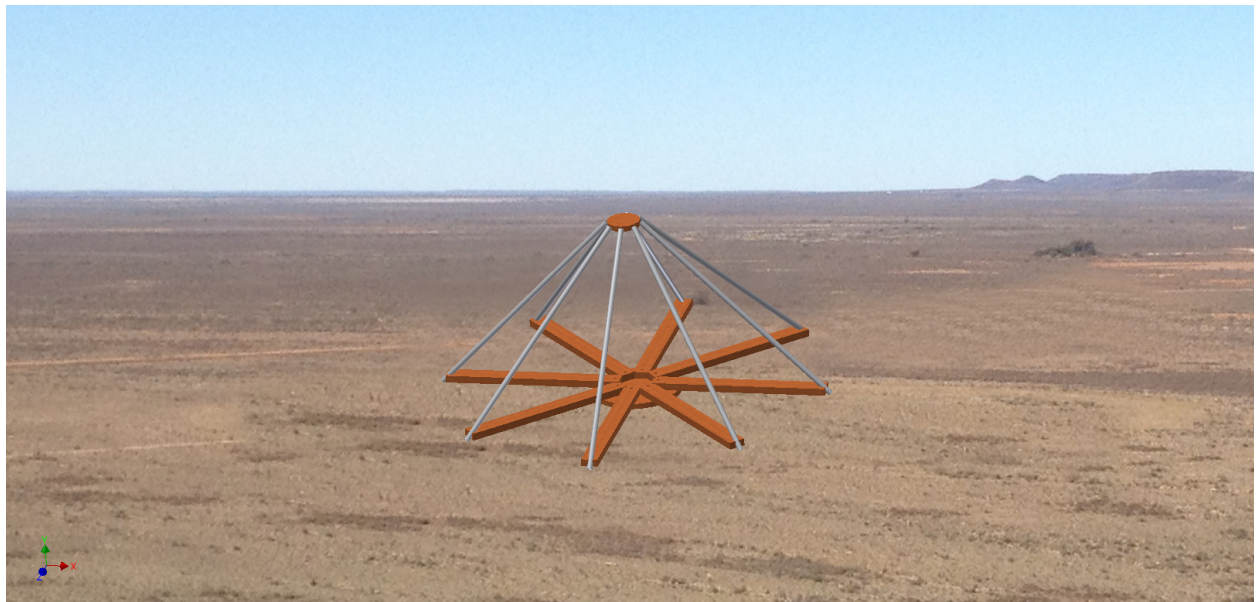


Fig. 4.— The cone structure is wrapped around with quarter inch mesh wire cloth and placed on top of the central hub centered on the vertex of the parabolic dish to reduce backlobes. This cone structure is used in the cone test, a slight modification may be applied for better backlobes reduction as suggested by the reflection measurements in the cone test.

4.5. hub

The central hub has an overall diameter of 37", the inner sono tube has an interior diameter of 18", the outer sono tube has an interior diameter of 36". The launch angle of the spar sleeves is $+2.86^\circ$ from the inner sono tube to the outer sono tube, the supporting sleeves (bottom sleeves) do not have any launch angles.

4.6. feed suspension

The feed suspension mechanism consists of a back plane made out of wire cloth and $\frac{3}{4}$ " schedule 40 white PVCs bolted on a metal hexagon, and a mast from the metal structure connects the dipole feed to the back screen. The whole feed structure is suspended above the hub by attaching kevlar wires from the three poles to the back of the metal structure.

Each pole has a reel with kevlar ropes wrapped, adjustments to feed height can be made by cranking the reels.

4.7. material, PVC selection

The dish structure is made out of schedule 40, white PVCs to minimize the bending effect under sunlight exposure; PVCs are subject to thermal contraction and expansion with a linear thermal coefficient of $50.4 \times 10^{-6} \frac{m}{m^\circ C}$.

- bent pipes as approximation to parabola
- faceting
- shielding
- splash cone
- hub
- feed suspension (feed with mast, back screen by kevlar wire)
- materials, PVC selection
- design lifetime (wood, PVC)

5. Simulated Performance

5.1. Beam Pattern

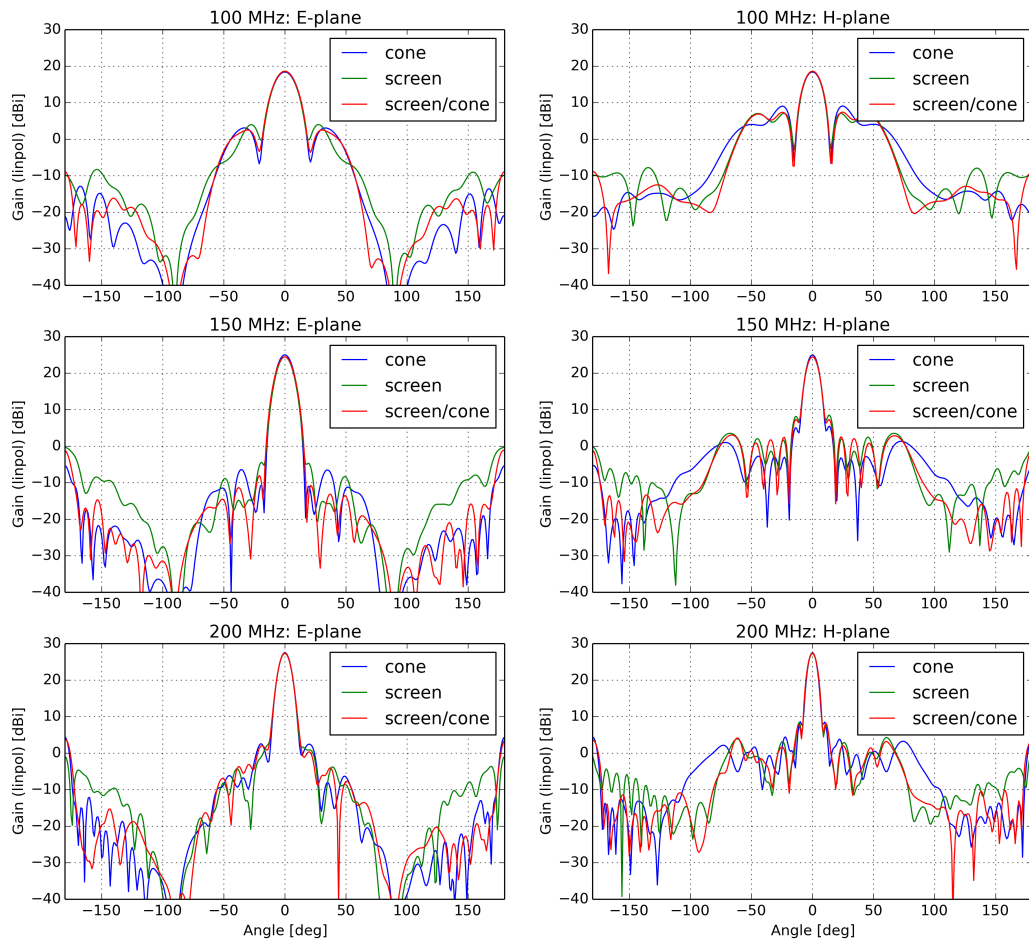


Fig. 5.— THIS FIGURE SHOWS THE BEAM PATTERN

- beam pattern
- delay performance (E-M modeling)

6. Fabrication and Deployment

- lessons/principles
- process to precision to specifications on precision

7. Time Domain Reflectometry

With the use of a vector network analyzer (VNA), time domain reflectometry is a technique that measures the magnitude and phase of a reflected signal, often referred to as S-parameter as function of time and frequency. The return loss of the reflection is dependent on the impedance of the device under test (DUT). The network analyzer provides a frequency swept signal and the inverse Fourier transform is then performed to produce reflection parameter measurements as a function of time.

S-parameter stands for "scattering parameters", the term is widely used to describe a device under test at any distance in network measurements provided that the transmission cable used is lossless, the magnitude remains constant when propagating down the cable. S_{ii} is analogue to optical reflection coefficient, and S_{ij} is analogue to optical transmission coefficient.

In a two port network that was used in the dish test, the incident wave (a_1, a_2) are independent variables, and the reflected waves (b_1, b_2) are the dependent variables used to define the S-parameters. a_i and b_i of the i^{th} port is related to the terminal voltage V_i , the terminal current I_i and a reference impedance Z_0 as follows:

$$a_i = \frac{V_i + Z_i I_i}{2\sqrt{|ReZ_i|}} \quad (2)$$

$$b_i = \frac{V_i + Z_i^* I_i}{2\sqrt{|ReZ_i|}} \quad (3)$$

and in terms of V_{inc-i} voltage incident on and V_{ref-i} voltage reflected from port i as follows:

$$a_i = \frac{V_{inc-i}}{\sqrt{Z_0}} \quad (4)$$

$$b_i = \frac{V_{ref-i}}{\sqrt{Z_0}}. \quad (5)$$

The relationship between the reflected and incident power at each port of a network can be described linearly as:

$$b_1 = S_{11}a_1 + S_{12}a_2 \quad (6)$$

$$b_2 = S_{21}a_1 + S_{22}a_2 \quad (7)$$

and in matrix representation:

$$\begin{pmatrix} b_1 \\ b_2 \end{pmatrix} = \begin{pmatrix} S_{11} & S_{12} \\ S_{21} & S_{22} \end{pmatrix} \times \begin{pmatrix} a_1 \\ a_2 \end{pmatrix} \quad (8)$$

When considering the incident power at port 1, the power can either be reflected on the same port as b_1 or be transmitted through port 2 as b_2 . When the output port (port 2) is terminated

with a matched load, S_{11} becomes:

$$\begin{aligned} S_{11} &= \frac{b_1}{a_1}|_{a_2=0} \\ &= \frac{\frac{V_1}{I_1} - Z_0}{\frac{V_1}{I_1} + Z_0} \\ &= \frac{Z_1 - Z_0}{Z_1 + Z_0} \\ S_{21} &= \frac{b_2}{a_1}|_{a_2=0} \end{aligned} \tag{9}$$

S_{11} , S_{22} are the input and output reflection coefficient respectively, hence they are a measure of the input and output mismatch loss. $|S_{11}|^2$ is the ratio of the reflected power from versus the incident power on the input port, $|S_{22}|^2$ is the ratio of that of the output port. S_{21} measures the forward transmission a.k.a the voltage gain and S_{12} measures the reverse transmission a.k.a the voltage gain. The square of S_{21} is the ratio of power delivered to a load with impedance Z_0 versus power available from source with Z_0 . Hence S_{12} and S_{21} are a measure of the insertion gain.

TDR measurements are often related to the reflection coefficient Γ [-1, 1] and the voltage standing wave ratio (VSWR), by definition:

$$\Gamma = \frac{V_{reflected}}{V_{incident}} \tag{10}$$

$$\begin{aligned} VSWR &= \frac{E_{max}}{E_{min}} \\ &= \frac{1 + \Gamma}{1 - \Gamma} \end{aligned} \tag{11}$$

where E_{max} and E_{min} are in reference to the envelop of the travelling wave.

—(Further Reference: G. Gonzalez, Microwave Transistor Amplifiers: Analysis and Design, Prentice Hall, 1984)—

When the VNA measures the S-parameters in the frequency domain, the data is measured across a pre-defined frequency range and stored at discrete points across this span. The frequency spacing between data points is proportional to the frequency span and inversely proportional to the total number of data points.

Time domain reflectometry (TDR) is carried out with the feed as the device under test after the mesh panels are installed. In this application, time domain reflectometry measures the reflections on the dish as a function of time as a result of impedance mismatch between the feed electronics and the sky signal. The characteristic impedance of the output signal from the vector network analyzer and transmission coaxial cable is 50Ω . The impedance of free space is $120\pi\Omega$, with the

use of a 4:1 passive balun at each polarization, the signal through the balun at the reference plane should have a characteristic impedance of $30\pi\Omega$. In practice, a third impedance in the system comes from the PAPER feed element itself and is simulated as $\sim 130\Omega$. In effect, the test has two devices under test in the network.

Each polarization is connected to a port on the vector network analyzer, the time axis represent the physical distance as the signals propagate along the transmission cables. The physical distance of can be related to the time axis using:

$$D = \frac{t}{2}v_{fac}c, \quad (12)$$

t is the round trip travel time as recorded as the time data. The VNA is calibrated at the end of the cables connecting the baluns, hence the velocity factor in the measurements can be taken as 1, resulting the speed of propagation to be the speed of light c , thereby 1 ns is equivalent to 29.98 cm in free space and approximately 1 ft from the passive baluns.

The expected reflection from simulation and mathematical derivation is -60dB by 2 reflections between the focal point and the vertex. The designed focal length of the dish is 4.5m, 2 times of reflection (i.e. 4 crossings attenuation) corresponds to 59.0 ns in time domain.

7.1. Choice of Hardware

The dual-polarization feed used in PAPER is implemented in this prototype, consisted of four sleeved dipoles, the crossed dipoles made from copper tubing are encased between two thin alminium disks(A. Parsons, 2008). A 4:1 passive balun is attached to the dipole through a mating board for each polarization, fixed-length 50Ω coaxial cables connect the baluns to the ports of a VNA for TDR measurements. The left drawing on Figure 6 demonstrates the electronic setup while performing the TDR measurements. The LMR400 coaxial cables of length 10 m has a signal attenuation of ~ 0.5 dB over 10 m at 150 MHz. The Aglient ES8753A is being used as the VNA to carry out the TDR measurements, the system dynamic range is 100 dB at 16 MHz to 3 GHz and the directivity is 55 dB at 300 kHz - 1.3 GHz, where the frequency range of interest is 50 MHz - 1 GHz.

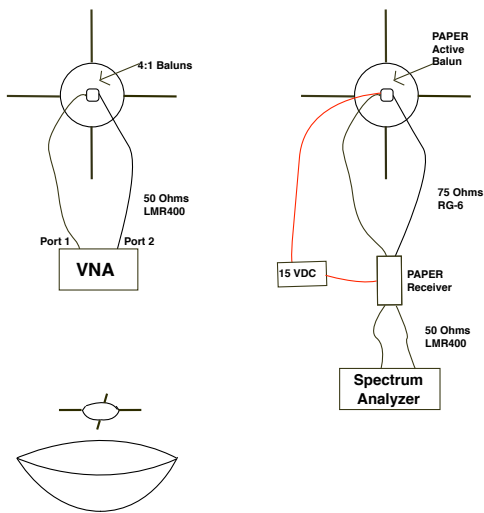


Fig. 6.— The drawing on the left shows the setup used for TDR measurements with the use of a vector network analyzer and two passive baluns. The drawing on the right is the setup used for sky test in Section 8.3, where the baluns are replaced by a PAPER balun. In any tests, the feed is hung up above the dish.

7.2. Calibration of VNA

Calibration is performed prior to taking measurements to eliminate the systematic effects caused by cables, adapters, and connectors. Performing calibration at the end of the cables shifts the reference plane to the SMA connectors of the cables that are connecting the baluns with zero phase, zero loss and zero mismatch; as such, the measurements taken are showing only the effects of the feed and baluns under different configurations. The full two port calibration is done by attaching the calibration standards (SHORT, OPEN, LOAD, and THROUGH) to the end of the 50Ω cables, the VNA calculates the correction coefficients and applies the coefficients subsequently to each measurements. The calibration coefficients includes offset delay, capacitance in the form of a fourth order polynomial, inductance as a fourth order polynomial, offset loss as resistance per second, and offset characteristic impedance.

The effect and significance of such calibration is shown in Figure 7. The blue curve shows that without calibration, systematic errors cause the response function to vary over frequencies when the end of the cables is opened, the red curve shows that with calibration, the measurements are what one would expect. In theory, S_{ii} of the i^{th} should be 0 dB and independent of frequency; zero return loss measured in dB corresponds to Γ being 1, no power was being transmitted, which is measured in the calibrated red curve.

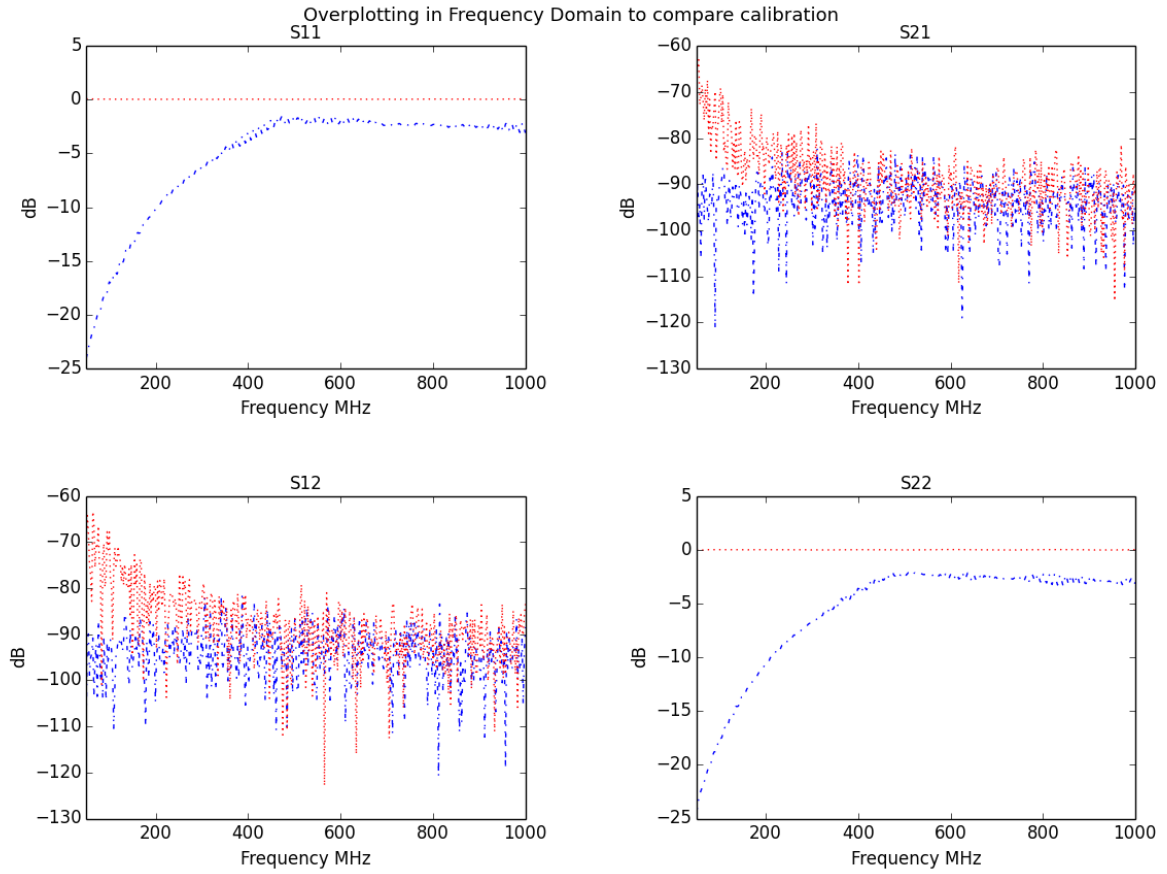


Fig. 7.— The reflection and transmission parameters of the full 2-ports are plotted as a function of frequency to show the significance of applying standard calibrations prior to taking measurements. The blue curves represent the uncalibrated results, and the red curves represent the calibrated results when the far cable ends were not terminated. The calibrated result shows a constant 0 dB over frequency as predicted.

A SHORT standard calculates the offset delay, offset loss, and specifies the inductance coefficients L_0 through L_3 to model the phase shift caused by the residual inductance in the standard as a function of frequency by fitting a forth order polynomial. An OPEN standard calculates offset delay, offset loss, and specifies the capacitance coefficients C_0 through C_3 to model the phase shift due to fringing capacitance as a function of frequency by fitting a forth order polynomial. The offset delay is the one way propagation time that can be obtained from speed of light in free space, the physical length and the permittivity constant of the cable material; the offset loss as a function of frequency is caused by the skin effect of offset coaxial type standards. During the calibration process, the SHORT standard and OPEN standard are off by 180° ; the reflection coefficients should be 1 (0 dB) at 0° , and 1 at 180° at all frequencies for OPEN standard and an ideal zero-length short respectively. A perfect LOAD standard should have a reflection coefficient of 0 as the characteristic impedance Z_0 matches the specified impedance on the network analyzer.

7.3. Configurations

The measurements are taken with 401 data samples between 50 MHz to 1 GHz, giving a time resolution of 1.05 ns; each set of data is averaged by 16 measurements for higher SNR. The first test being carried out is by varying the feed height above the vertex, and the second test is by placing a splash cone on the central hub centered on the vertex of the parabolic dish. The feed height test was carried out at three different heights above the dish: 67", 10'3.5", and 14'0.5" to verify the effect of reflection as a function of time delay which is directly related to the travelled distance of a signal and the number of crossings attenuation. The cone test was carried at a distance 14'6" above the vertex to investigate the backlobes of the antenna and the effectiveness of reducing the backlobes by placing the splash cone structure as shown in Figure 4.

7.4. Window Functions

To deal with real-life situations of a finite bandwidth which results in spectral leakage in time domain, a window function is applied to the frequency domain data prior to performing the inverse Fourier transform in order to increase the dynamic range of the measurements and minimize the effect of leakage in time domain by reducing the sidelobe levels; the disadvantage however, is the widening of the pulse width between data points hence reducing the time resolution.

As shown in Figure 8, the spectra features are emphasized by multiplying a window function to the frequency response prior to performing the inverse Fourier transform to time domain. By varying the β value of a Kaiser-Bessel window or by choosing different window functions, such as the Blackman-Harris window (cyan) give different side-lobe levels, as shown in the time range 200 - 300 ns. The default window function used in the TDR analysis throughout this document is the Blackman-Harris. The strong reflection peaks to the left of 40 ns is caused by impedance

mismatch along the signal path in the connectors, the mating board, and more importantly, from the impedance of the feed itself.

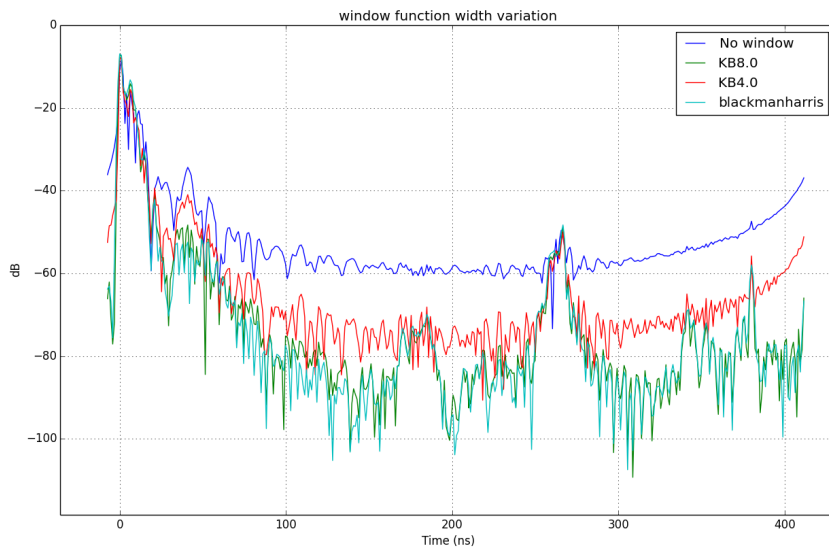


Fig. 8.— Spectra with different window functions applied prior to taking the inverse Fourier transform is plotted against the spectrum without multiplying by any window functions. The dynamic range increases as the side-lobe levels is weighted by the specified amount in a function while retaining the spectrum features.

- reflectometry
- hardware
- calibration of the good
- feed height test
- configurations
- window function used in delay transform

8. Results

8.1. Delay Spectrum for Configurations

The time axis shows the delay in nanoseconds as the signal propagates starting from the calibrated reference plane: the SMA connectors at the far ends of the cables. When the signal first contact the connectors on the balun, the mating board, and the feed, the signal is not masked by reflections caused by any components between the connectors and the reference plane, as demonstrated by the strong reflection peaks between 0 ns - 30 ns. When the signal continues to propagate after the first reflection, the power is reduced from the original pulse as the first impedance mismatch caused some of the power to be reflected back as opposite to being fully transmitted.

All the traces in Figure 9 show that there are two large peaks representing the reflections from the mountains nearby, the black curve in the figure was measured while the feed was resting at ~60 ft from the dish, and those two peaks shifted in time accordingly.

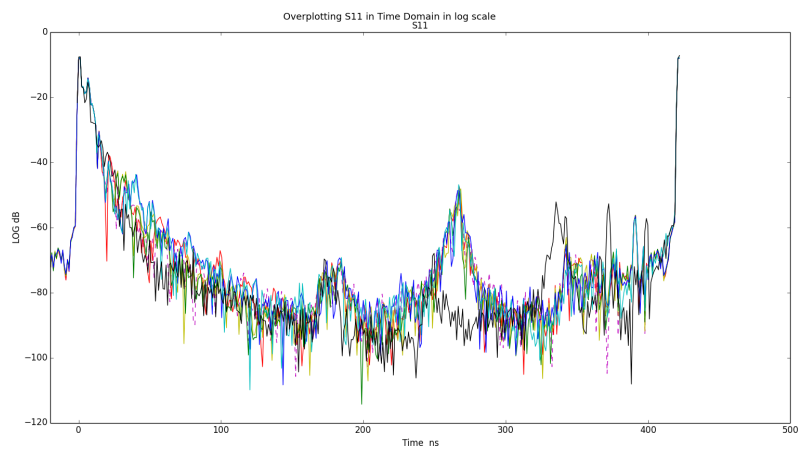


Fig. 9.— S_{11} of the height test, performed while the feed was hanging at height : 67", 10'3.5", and 14'0.5" above the vertex. The black curve represents the S_{11} measurement as the feed was located at ~ 60 ft from the dish, hence the peaks at ~ 260 ns and ~ 330 ns implies that they are the reflections due to surrounding mountains.

Intuitively, the peaks associated with the connectors and surrounding environment should be unshifted in time as the feed height varies, as these components were static during the measurements. Figure 10 shows the time domain response when the feed is positioned at 67”, 10’3.5”, and 14’0.5” above the vertex, raised by 4’ from the preceding, 4.5 m is the focal length of the 14 m parabolic dish with $\frac{f}{D} = 0.32$. By 59 ns, as required in the antenna design, the S_{11} is down by -61.7 dB excluding the reflection peak caused by the mountains as shown in Figure 9.

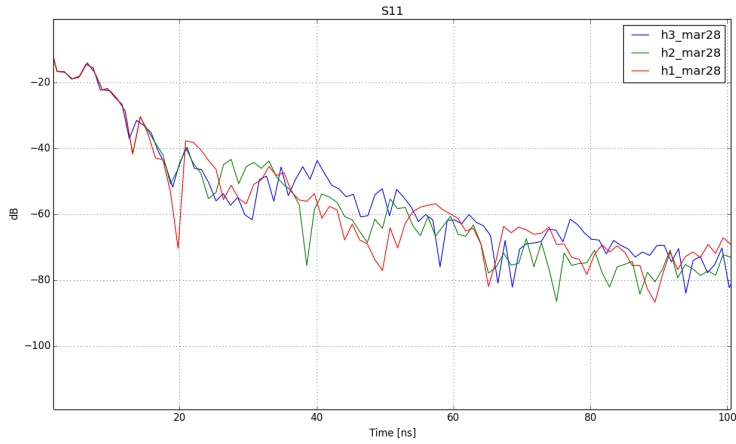


Fig. 10.— The time domain response changes when the feed is positioned at 67”, 10’3.5”, and 14’0.5” above the vertex. The red curve represents the response taken at height 67”, this curve has the highest peak amplitude, followed by the green curve, taken at height 10’3.5” and lastly the blue curve, taken at height 14’0.5” (the ideal focal distance of the parabolic dish). By 59 ns, as required in the antenna design, the S_{11} is down by over -61.7 dB excluding the reflection peaks caused by the mountains.

8.2. Cone test

VNA measures the time responses of when the cone is placed on the central hub versus when the cone was absence as the feed was at height 14'6" in both setups. The measurements in Figure 11 show that the placement of the splash cone reduces the backlobes in the response up to ~ 48 ns, at which the power is down by -55 dB.

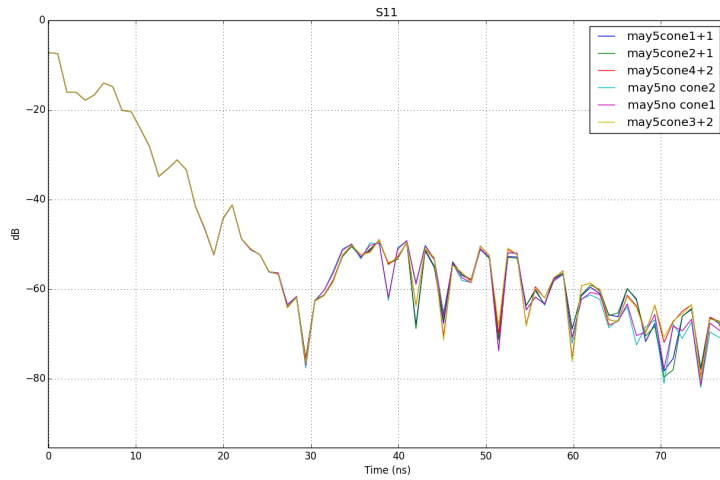


Fig. 11.— The above shows the difference in time response when the feed was at 14'6" above the vertex, the vertex was covered by the splash cone versus the vertex was not covered. Up to ~ 48 ns, the measurements suggest that the cone reduces the backlobes, and by 59 ns, the response is down by -59.9 dB.

8.3. RFI investigation

To measure the spectra of the sky with the prototype, the dipole element is connected to the PAPER active balun which has a total amplification of ~ 32 dB for the signals from both polarizations and outputs analog signals through fixed-length RG-6 75Ω coaxial cables into the PAPER receiver. The receiver contains two 100-200MHz bandwidth filters, and outputs 50Ω signals after amplification with gain $\sim XX$ dB. The 50Ω signals travel along the LMR 400 cables to the Agilent E4407B spectrum analyzer. The spectra are taken with 401 data points, ranging from 100 - 200 MHz, and 50 measurements are averaged to improve the SNR, the resolution bandwidth is specified to be 1 MHz with 0 dB attenuation, and the resulting spectra has a resolution of 0.25 MHz.

Cygnus A, a radio bright source is at right ascension $19h59m28s$ and declination $+40^\circ 44'02''$ and the dish is located at $+37.98^\circ$ latitude, and -122.19° longitude. Cygnus A, hence is an ideal source for the sky test as it transits at night time during the summer when observations are carried out. Three spectra shown in Figure 12 are taken at different times in a day: daytime, before and during the transit of Cygnus A in our beam during the nighttime.

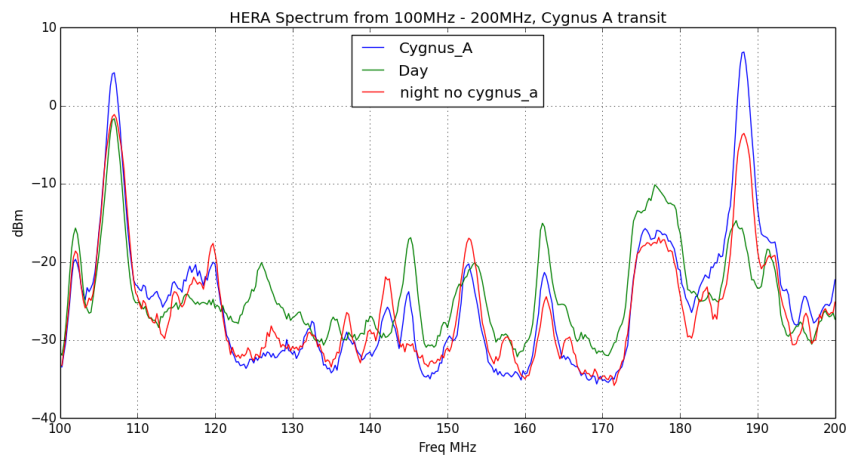


Fig. 12.— Three spectra taken at different times in a day spanning the frequency range from 100 MHz to 200 MHz. Radio stations and TV broadband channels are the major RFIs in the vicinity of our dish. During nighttime, as shown by the blue and red curves, the beam pattern can be studied by observing the power of a radio bright source throughout the night in those narrow channels with minimal RFIs.

Spectra in Figure 13 are taken at nighttime, approximately 4 hours before Cygnus A transits within the beam to ensure uncontaminated frequency channels can be effectively identified. As the resolution bandwidth is reduced from 1 MHz to 1 kHz and the averaging number of measurements is reduced to 0, channels with minimal RFIs are identified as 120 - 130 MHz, 155 - 160MHz, 165 - 175MHz and color plotted as green, red, and cyan respectively in Figure 13.

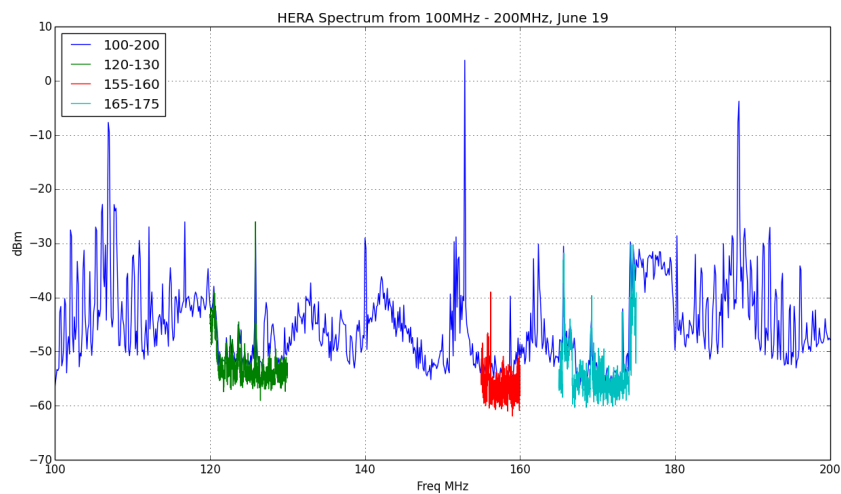


Fig. 13.— The narrow channels with minimal RFIs are identified as 120 - 130 MHz, 155 - 160 MHz, and 165 - 175 MHz. The power in dBm are lower than the spectra shown in Figure 12 as the resolution bandwidth is reduced from 1 MHz to 1 kHz.

Spectra are taken in those frequency channels every 10 ± 2 minutes throughout a night as Cygnus A rises and transits across the beam. Figure 14, and 15 show that within these narrow channels that were identified according to the 100-200MHz spectra, RFIs were present occassionaly throughout the observing night; hence, narrower channels within the spectra are extracted to calculate the power as a function of altitude and local sidereal time.

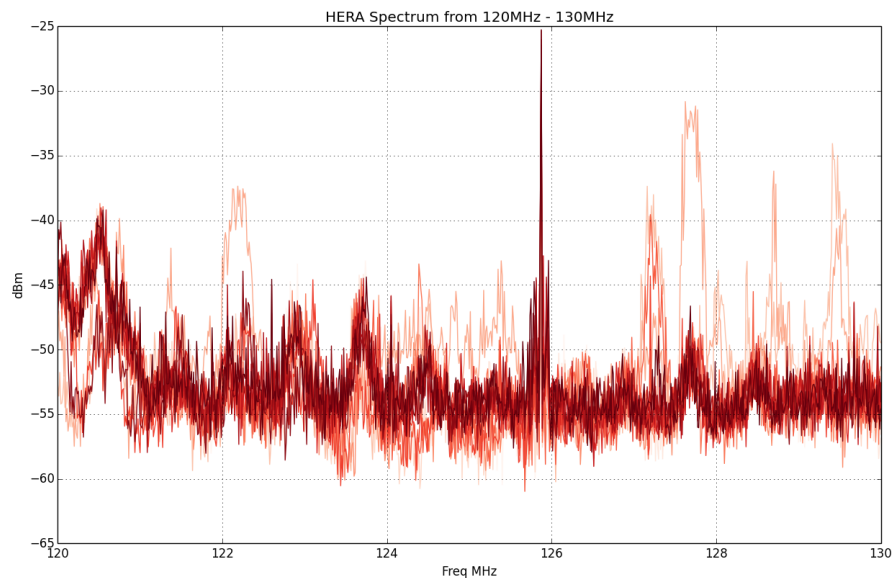


Fig. 14.— Here, the spectrum running from 126 MHz to 127 MHz is the quiet region within the 120 - 130 MHz channel that was chosen according to the 100 - 200MHz nighttime spectrum shown in Figure 13.

blah blah blah blah blah

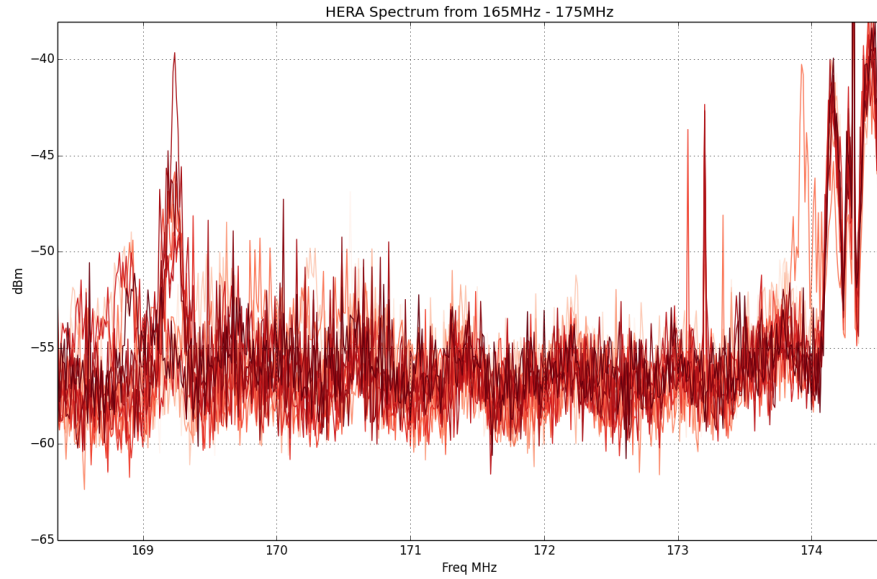


Fig. 15.— Here, the spectrum running from 171 MHz to 173 MHz is the quiet region within the 165 - 175 MHz channel that was chosen according to the 100 - 200MHz nighttime spectrum shown in Figure 13.

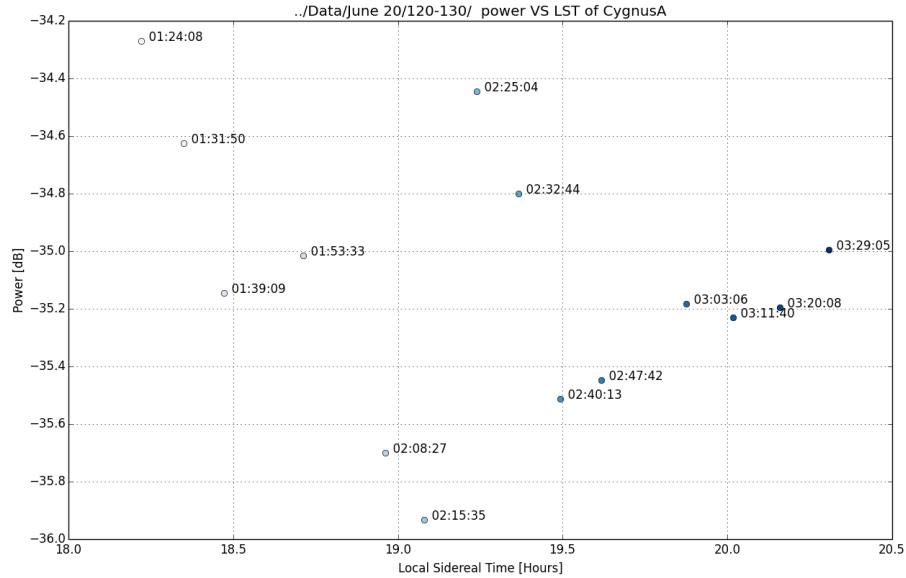


Fig. 16.— 126-127 LST

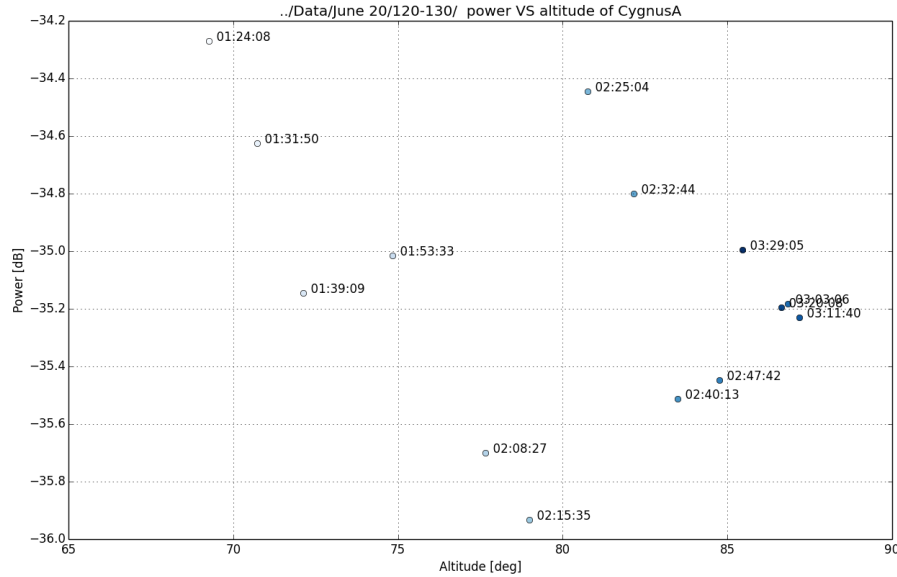


Fig. 17.— afga

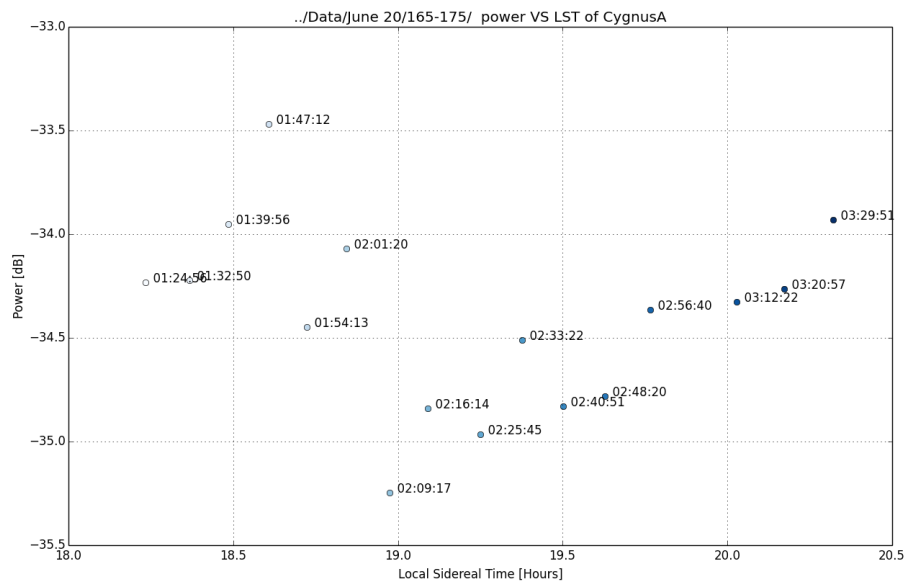


Fig. 18.— 171-173 LST

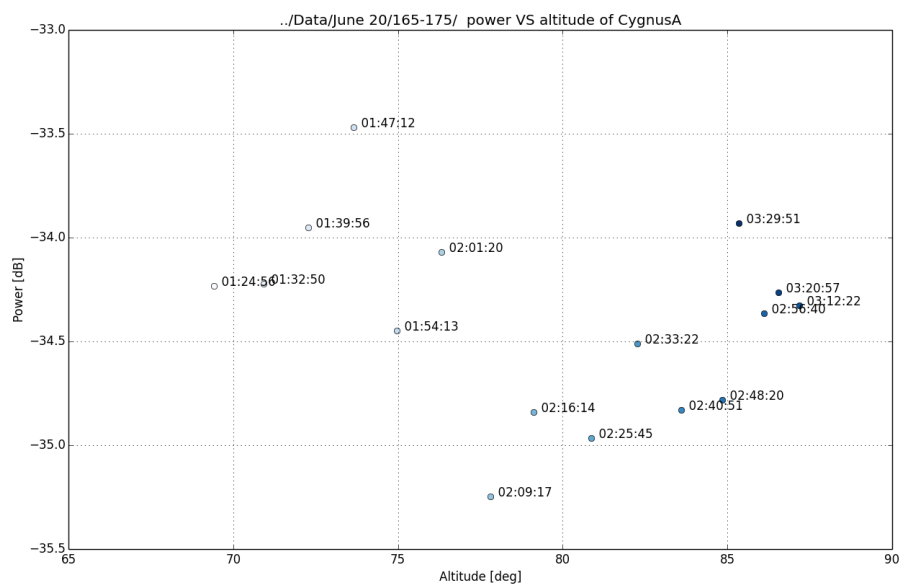


Fig. 19.— 171-173 alt

8.4. How well did we place everything

stringent parameters that affect the overall parabolic dish surface error, geometry of rays, -the hub is centered at the vertex within couple inches....

Resurvey the center for hub after telephone poles were stabilized in the ground. The telephone poles have varying diameter and along the length.

The surrounding posts are not equidistant to the center of the hub; within 5' between maximum post to center distance and minimum post to center distance.

The survey points in the table is defined as: Pole 1 = the very first pivot pole, hand drilled hole; Pole 2 = The highest pole near the fence; Pole 3 = the pole closes to the shed, near where our cars are parked

Point 1	Point 2	Distance
Pole 1	Pole 2	48' $\frac{1}{4}$ "
Pole 1	Center	332"
Pole 1	Pole 3	47' $\frac{2}{3}$ "

Table 1: The table lists the distances between poles and center before drilling the 2 holes after locating the point of same horizon using a theodolite and 2X4s .

We measured the pole to pole distance after the center is finalized at the same height on all poles.

Point 1	Point 2	Distance [Feet]
Pole 1	Pole 2	47.1
Pole 2	Pole 3	47.4
Pole 1	Pole 3	46.9

Table 2: The table lists the distances between poles after we finalized the center.

ideal parabola: simulated parabola: real life parabola:

- delay spectrum for configurations
- cost
- photos of constructed element
- XXX hook up receiver and to a sky test — what is XXX?
- measured parabolicity — Total station?
- why were we right in the attenuation per reflection?

- does the cone help?
- how well did we place everything?
- ways to ensure spec in field
- mention extender as unnecessary in flat deployments

9. Conclusion

- relevance to HERA, project cost
- link Pober et al. (2014) sensitivity/science
- polarization matching
- frequency coverage, need for a feed re-design.

10. Acknowledgment

We would like to thank SKA-SA for the site infrastructure, maintenance, and observing support that has made this work possible, as well as the significant efforts of the staff at NRAO’s Green Bank and Charlottesville sites. AP would like to thank M. McQuinn and A. Lidz for helpful discussions and ionization models. The PAPER project is supported by the National Science Foundation (awards 0804508, 1129258, and 1125558), and a generous grant from the Mt. Cuba Astronomical Association.